ELSEVIER

Contents lists available at ScienceDirect

## Materials Today Nano

journal homepage: https://www.evise.com/profile/#/MTNANO/login



# Polarization optical switching based on the molding of coherent light scattering via surface lattice resonances



Seyed M. Sadeghi <sup>a, \*</sup>, Rithvik R. Gutha <sup>a, 1</sup>, Sean Ramsay <sup>a</sup>, Dustin Roberts <sup>a</sup>, Christina Sharp <sup>b</sup>

- <sup>a</sup> Department of Physics and Astronomy, University of Alabama in Huntsville, Huntsville, AL, 35899, USA
- <sup>b</sup> Department of Physics and Astronomy, University of Exeter, Exeter EX4 4QD, United Kingdom

#### ARTICLE INFO

Article history:
Received 19 November 2021
Received in revised form
21 December 2021
Accepted 25 February 2022
Available online 3 March 2022

Keywords: Plasmon Mulitpolar resonances Collective Scattering Plasmonic lattices

#### ABSTRACT

We study the molding of coherent light scattering in the planes of Au metallic nanoantenna arrays (inplane light scattering) using surface lattice resonances. The nanoantennas are considered to have similar periodicities and footprints (lateral shapes and sizes) but their heights are varied from 20 to 80 nm. We measure the spectra and relative intensities of the scattered light along the edges of the substrates supporting periodic arrays of such nanoantennas. Our results show that in the case of nanoantennas of high degree of flatness (20 nm height), the variation of the incident light polarization can lead to binary partition of scattered light energy between two modes at two different wavelengths, offering a polarization optical switching process in the near infrared range. This happens as the nature of the light scattering process changes from plasmonic to coherent diffraction associated with the formation of "edge-mode' surface lattice resonances. As the heights of the nanoantennas are increased, the energy transfer process becomes more continuous, offering mixture of the two scattering processes.

 $\ensuremath{\text{@}}$  2022 Elsevier Ltd. All rights reserved.

#### 1. Introduction

Plasmonic surface lattice resonances (SLRs) occur when metallic nanoantennas are arranged in a periodic way, fulfilling the Rayleigh Anomaly (RA) condition. Under this condition, the scattered field propagates in the plane of the array, coupling localized surface plasmon resonances in-phase. SLRs have been used to activate the subradiant plasmonic modes of nanoantennas via their coupling with the lattice modes [1-3]. They offer a wide range of applications, ranging from biological and chemical sensing [4-9], to excitonic laser systems [10-12], optical filters [13], control of the emission of quantum emitters [10,12], perfect absorbers [14], and quantum information applications [15]. It has been shown that the optics of periodic structures and RA coupling can also be applied to periodic arrays of regions containing densely-packed Au nanoislands, forming plasmonic networks [16]. Under these conditions, the strongly localized plasmon fields of the nanoislands become delocalized in each region while diffraction couples these regions

coherently along a given direction. The RA coupling can also excite a plasmonic network containing long arrays of nanoantennas with random shapes and sizes, supporting lattice-induced plasmonic dipole antennas excited in phase [17].

Significant attention has been paid to understand the impact of shapes and sizes of nanoantennas on the formation of SLRs [1]. It has been shown that such resonances can be more prominent in homogeneous media, although they can also occur efficiently in inhomogeneous environment when the plasmonic polarizability of nanoantennas is sufficiently large [7,18]. A relatively less studied case, however, is the formation of SLR in arrays of flat metallic nanoantennas (FmANTs). Such structures refer to the cases wherein the lateral dimensions of the metallic nanostructures are much larger than their heights. In such structures, plasmonic resonances fall into two different categories, called edge and cavity modes [19-22]. The former happens at the edges of the structures while the latter at their centers [19,23]. The bonding and antibonding modes of FmANTs and their coupling to RA, i.e. formation of SLRs, have recently been investigated [21,24,25] Applications of such SLRs for chemical and biological sensors [8,26], and the impact of their shapes [27-30], and material compositions of FmANTs [31,32], have also been investigated.

<sup>\*</sup> Corresponding author.

E-mail address: seyed.sadeghi@uah.edu (S.M. Sadeghi).

<sup>&</sup>lt;sup>1</sup> Current address: II-VI Photonics Inc. Paignton, UK.

In this article, we investigate the control of the grazing (inplane) light scattering in arrays of FmANTs via SLR as the degree of the flatness and polarizability of nanoantennas are changed. For this, we fabricated arrays of FmANTs that have similar lateral footprints (shapes and sizes) and lattice constants ( $a_x$  and  $a_y$ ) but their heights (H) are increased from 20 to 80 nm, depicting various degrees of flatness and plasmonic polarizability (Fig. 1a and b). We directly measure the scattered light propagating along the plane of such arrays using an optical setup that allows us to spectrally map the light reaching the edges of the samples at different locations (Fig. 1c). Using this, we study the impact of the formation of SLRs associated with such FmANTs ("edge-mode' SLRs) as the incident light polarization is varied. Our results suggest significant variations in the in-plane light scattering as the heights of FmANTs are changed. The most prominent case occurs for the very thin FmANT (H = 20 nm), wherein our results show as the incident light polarization is changed from x-axis to y-axis (Fig. 1c), the scattered light undergoes a discrete wavelength shift. Under these conditions, the energy is efficiently partitioned in binary fashion between two modes, one associated with plasmonic scattering and the other with "edge-mode' SLR. This offers an optical switching process in the near infrared wavelength, wherein the incident light polarization can be used to determine the ratio of the energy transferred into these two modes. We show as the degree of flatness decreases, i.e. H increases, transition between these two modes becomes non-discrete, indicating a continuous wavelength shift and mode mixing.

The results of this article offer unique perspective of the far-field scattering caused by edge-mode plasmon resonances and the SLRs caused by the diffractive coupling of such resonances. Polarization switching of such scattering between two distinct modes with small spectral overlap without any need for complicated optical setups can be useful for integrated photonic devices. The results of this article can also have applications in optically pumped laser systems based SLRs, nano-scale spectroscopic systems, sensors, and design of optical feedback for planar cavity systems in on-chip passive/active devices [33—35].

## 2. Methodology

E-beam lithography techniques were used to fabricate four types of samples consisting of arrays of FmANTs on glass substrates with side dimensions of 22 mm and thicknesses of 0.2 mm. The specifications of the FmANTs are shown in Table 1, wherein  $L_x$  and  $L_y$  refer to the length of the x- and y-axes, respectively. For all

**Table 1** Lengths of FmANTs along the x-axis  $(L_x)$  and y-axis  $(L_y)$  in samples 1—4. H refer to the heights of these samples.

	$L_x$ (nm)	$L_y$ (nm)	H (nm)
Sample 1	840	220	20
Sample 2	830	218	40
Sample 3	890	250	60
Sample 4	850	215	80

samples, the lattice constants along the x-axis  $(a_x)$  and y-axis  $(a_y)$ were 1 and 0.5  $\mu$ m, respectively (Fig. 1a). The heights of the samples (H), however, were considered to 20 nm (sample 1), 40 nm (sample 2), 60 nm (sample 3), and 80 nm (sample 4). SEM image of one of the sample 4 is shown in Fig. 1b. The extinction spectra were measured using a transmission setup consisting of a Tungsten-Halogen lamp, polarizer, microscopic objective, and collective lens (Fig. S1, Supporting Information). Samples were placed between the objective and collective lens which directed part of the transmitted light toward visible and infrared spectrometers (Ocean Optics TE-cooled QE-Pro and FLAME) using fiber optics. The collective lens was placed at a sufficient distance right beneath the microscope objective to ensure a well-defined and small angle spread of illumination. To study planar light scattering through the substrates of the samples, we used an optical setup as shown in Fig. 1c. A microscope objective (2) was used to focus the light on the sample and another objective was placed close to the edge of the sample (1). The latter was on a translation stage, allowing it to move parallel to the edge of the substrates, along the x-axis. In addition to these, we used a microscope with dark field filter to study back the scattering of these samples under different cone half

Fig. 2 shows the extinction spectra of samples 1 (Fig. 1a), 2 (Fig. 1b), 3 (Fig. 1c), and 4 (Fig. 1d) when the superstrate was air (solid lines) or methanol (dashed lines). The results show that for the case when the polarization of the incident light is along the y-axis (y-pol), there is a common dominant peak in each spectrum (peaks  $A_1$ ,  $A_2$ ,  $A_3$ , and  $A_4$ ). As H increases, the wavelength of these peaks do not change significantly, but a side mode at the shorter wavelength side is developed ( $c_1$ ,  $c_2$ ,  $c_3$ , and  $c_4$  peaks). In case of sample 4 (Fig. 2d), this peak ( $c_4$ ) is quite distinct. In the case of sample 1, changing the refractive index of the superstrate by adding methanol with refractive index of ~1.322 leads to small amount of red shift (Fig. 2a, dashed line). For samples with higher H, however, this process leads to more complicated spectral changes. These

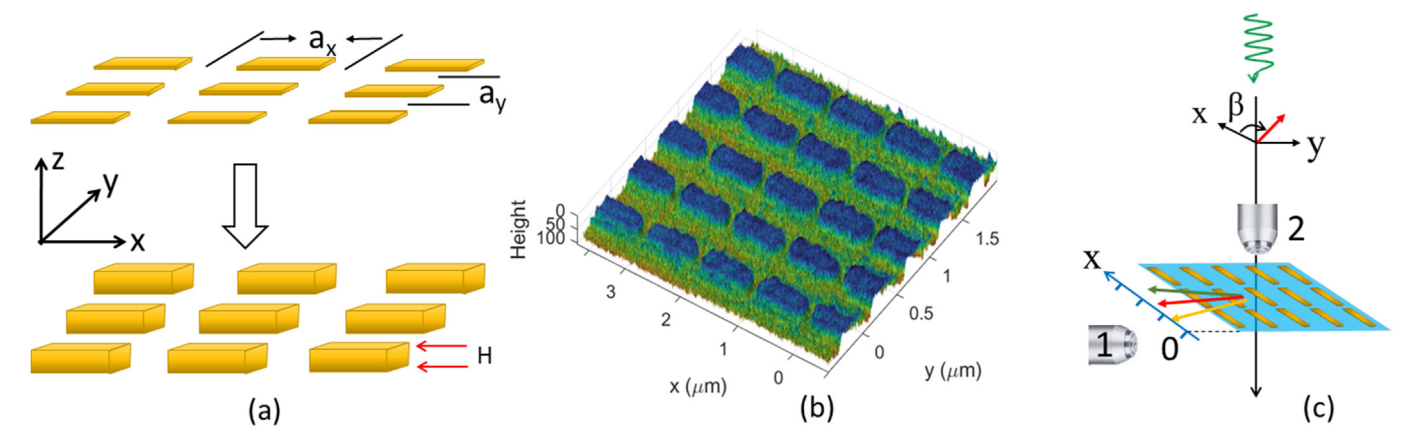


**Fig. 1.** (a) Schematic presentation of arrays of FmANTs with various heights. (b) An oblique view of SEM image of the array of FmANT with 80 nm height. (c) Optical setup for measurement of in-plane light scattering by FmANT array. Here  $\beta$  refer for the angle of polarization of incident light with respect to x-axis. FmANT, SEM.

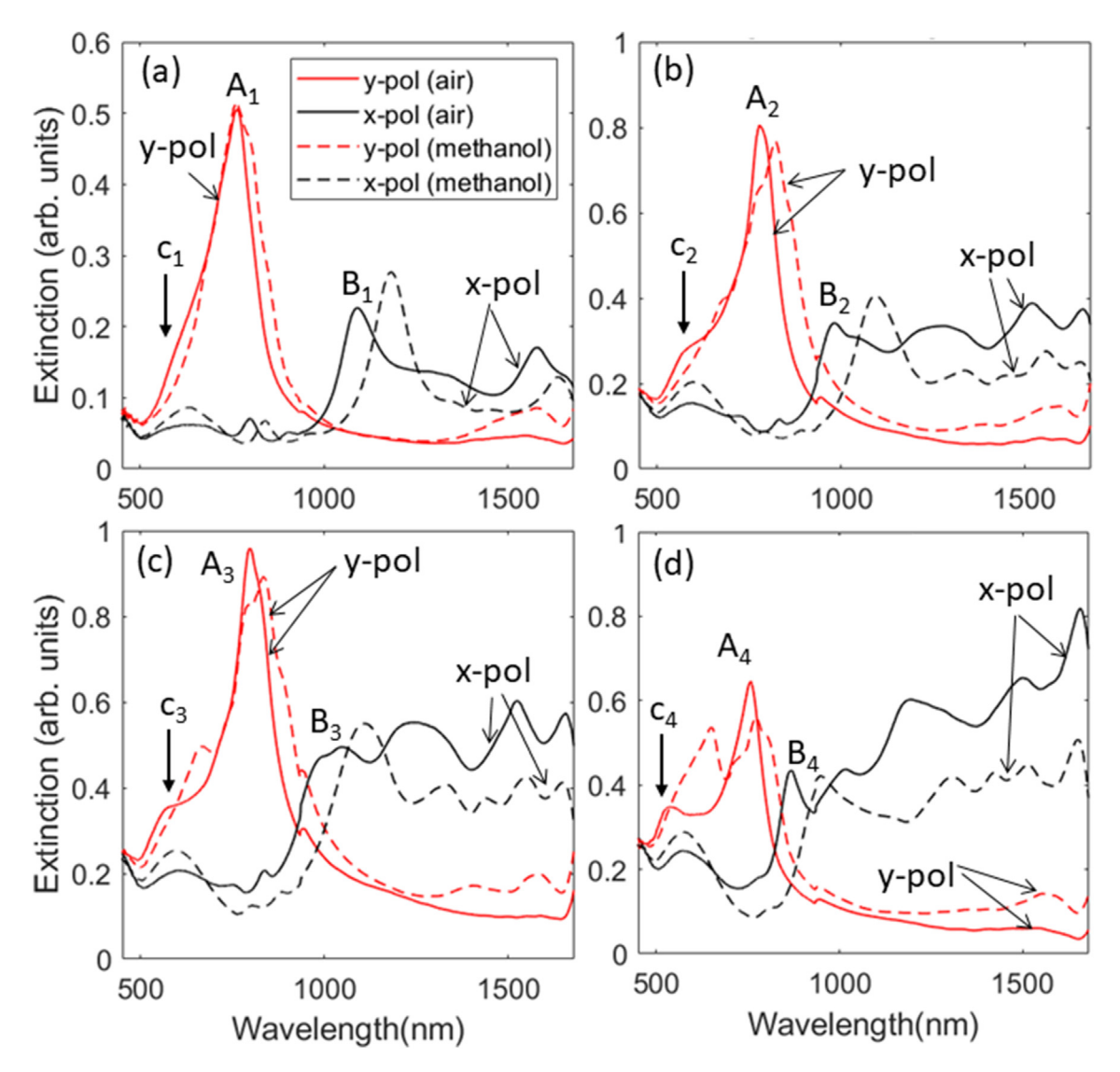


**Fig. 2.** Extinction spectra of samples 1–4 ((**a**), (**b**), (**c**), (**d**)) for x-pol and y-pol when the refractive index of the superstrate is air (solid line) and methanol (dashed line). Here, the red lines refer to y-pol and the black lines to x-pol. (For interpretation of the references to color in this figure legend, the reader is referred to the Web version of this article.)

include enhancement of the amplitudes of the peaks occurring at the shorter wavelength sides of the main peaks. This can be seen clearly for the case of samples 3 and 4 (Fig. 2c and d), i.e. peaks  $c_3$  and  $c_4$ . The much higher red shift of these peaks, than those of the main peaks  $(A_1-A_4)$ , can be associated with the plasmon modes that are deeply penetrated in the superstrate. In the cases of peaks  $A_1$ - $A_4$ , the plasmon modes are mostly localized in the substrates [24].

The results for the case when the incident light is polarized along the x-axis (x-pol), however, show significant changes in the plasmonic responses of the arrays as H increases. For the case of sample 1 (Fig. 2a), i.e. H=20~nm, the prominent peak (peak  $B_1$ ) occurs at about 1100 nm. As H increases, this peak is blue shifted to 977 ( $B_2$ , sample 2), 995 ( $B_3$ , sample 3), and 866 nm ( $B_4$ , sample 4) while multipolar resonances with different orders become evident (Fig. 2c and d). In fact, for the case of sample 1, we mostly see two main resonances, while for the case of sample 4, the number of the optically visible modes increases to 5. These results show how the thickness of FmANTs influences the edge plasmonic modes. For thinner FmANTs, the number of modes is less and they are quite distinct. As H increases and, therefore, the volumes of the nanoantennas become larger, higher order modes are excited. In fact in

the case of sample 1, the most significant peak for x-pol is peak B with amplitude of about 1/3 of peak A. For the case of sample 4, however, the most pronounced peak occurs at about 1650 nm with the amplitude of extinction more than that of peak A of the same sample (Fig. 2d). The impact of variation of refractive index (dashed lines) is also shown for the case of x-pol. The results show red shifts of the spectra, as expected. Note that the variations of  $L_x$  and  $L_y$  (Table 1) influence the transverse and longitudinal edge modes of the FmANTs, respectively. For the case of the transverse modes, the impact of these are convoluted by their coupling to the lattice modes. For the case of the longitudinal modes, the variations of  $L_x$  can influence the multi-polar nature of the edge modes.

To analyze back scattering of light from these samples, we measured their dark field scattering spectra. In general, in such a microscopy technique, the scattered field emitted into the angular cone of the detection optics strongly depends on the microscope objective [36–38]. Therefore, although the spectra is representative of the total scattered field of the nanoantennas, depending on the angle of incident light, plasmon modes can couple to light differently [36]. Considering these, in Fig. 3, we present the results for the back scattering spectra for samples 1 and 4 using microscope

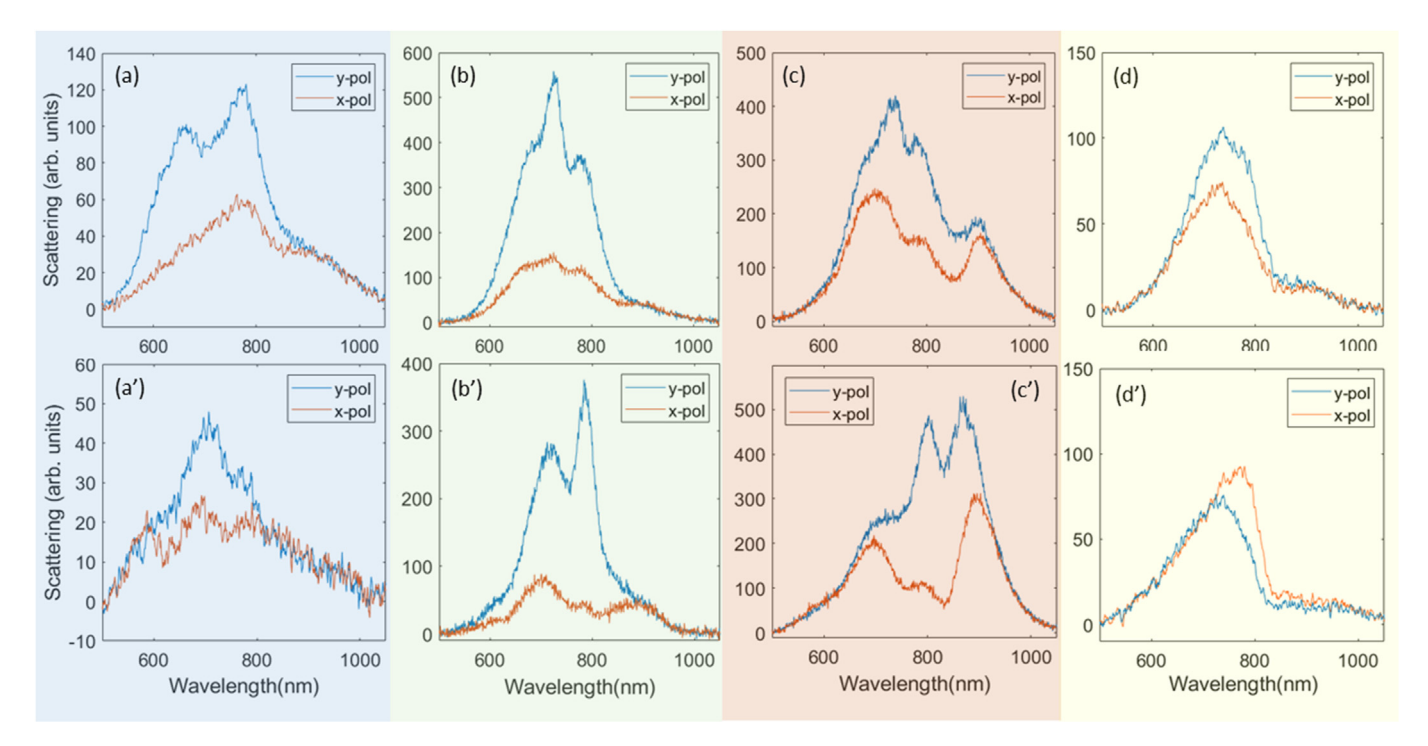


Fig. 3. Dark field back scattering spectra of samples 1 and 4 using objective with magnification of 10x ((a) and (a')), 20x ((b) and (b')), 50x ((c) and (c')) and 100x ((d) and (d')), (a)—(d) are for sample 1 and (a')–(d') are for sample 4.

objectives with magnifications of 10x (Fig. 3a and a'), 20x (Fig. 3b and b'), 50x (Fig. 3c and c') and 100x (Fig. 3d and d'). The numerical apertures (N.A.) of these objectives were, respectively, 0.3, 0.4, 0.7, and 0.99. The results suggest more distinct differences for the cases of x-pol and y-pol when microscope objectives with 10x, 20x, and 50x are used.

For the case of the 100x objective, samples 1 and 4 seem to support mostly similar spectra. The main differences include higher scattering for the y-pol than x-pol in case of sample 1 (Fig. 3d). In case of sample 4, this is vice versa (Fig. 3d'). On the other hand, for the case 50x objective, the results for y-pol and x-pol are quite different in these samples. For y-pol, for example, scattering in sample 1 is more efficient around 750 nm (Fig. 3c), while in sample 4, this occurs with a distinct doubling at longer wavelength range (Fig. 3c'). The results, for the case 10x and 20x, are also quite different. These results suggest that the heights of the FmANTs, i.e. degrees of their flatness, do not have significant impact on their back scattering when they are excited at very oblique angles (100x with N.A. = 0.99). For smaller magnifications (smaller N.A.), however, the heights of FmANTs draw significant differences, as seen in Fig. 3a-c and 3a'-3c'. This suggests that the edge modes are efficiently influenced by the components of the incident light wavevector along the z-axis (Fig. 1a).

## 3. Evolution of SLR with flatness and polarizability

To explore light diffraction and SLRs in the presence of different degree of flatness and polarizability, we rotated the samples along x- (x-rot) and y-axis (y-rot) for both x-pol and y-pol (Fig. 1a). Rotating lifts RA degeneracy, exposing the dark modes which are not seen at normal incidence. This allows us to characterize SLRs associated with different flatness and reveals dark and bright localized surface plasmon resonance modes. The angle of rotation is defined as the angle between the incident light direction (z-axis) and normal of the planes of arrays. For the cases of x-rot and y-rot, these angle are denoted by  $\theta_x$  and  $\theta_y$ , respectively.

To start, we consider the case of y-rot and x-pol. Under these conditions, since we align the light polarization along the x-axis, we are mostly dealing with the longitudinal plasmon modes. The results in Fig. 4a shows that, under these conditions, for the case of sample 1 when  $\theta_y=5^\circ$ , the main peak (peak B<sub>1</sub>) is red shifted. This happens with the optical activation of a dark mode (peak d<sub>1</sub>) and enhancement of an infrared peak (peak i<sub>1</sub>). For the case of  $\theta_y=10^\circ$  (Fig. 4a'), we see these peaks undergo more amplitude enhancement. For samples 2 and 3 (Fig. 4b-b" and Fig. 4c-c") similar features can be seen, except for the dark modes (d<sub>2</sub> and d<sub>3</sub>) which become less prominent. For the case of sample 4, this mode (d<sub>4</sub>) completely disappears with rotation (Fig. 4d-d"). In all cases when  $\theta_y=25^\circ$ , higher order modes appear while the amount of extinction is suppressed. The results do not suggest any sign of SLR, i.e. removal of RA degeneracy.

In contrast to the case of Fig. 4, if one keeps the polarization of the incident light polarization unchanged (x-pol) but rotates the samples along the x-axis (x-rot), the results offer a different picture. Under these conditions, the spectral variations are mostly limited to some small amount of blue shift for peaks  $i_1$  and  $i_4$  followed by amplitude suppression (Fig. S2, Supporting Information). For the case of peak  $B_1$ , however, the results suggest some red shift and its merging with a broader mode seen at longer wavelength. Similar to the case of Fig. 4, we do not see any significant sign of doubling associated with SLR. No dark mode activation can also be seen. A key difference between rotation along x and y-axes, is that the latter can efficiently activate the longitudinal plasmon modes of the FmANTs, while the former does not support such a process.

When the samples are rotated along the x-axis (x-rot) and polarization of the incident light is along y-axis (y-pol), the spectra changes drastically. As seen in Fig. 5, here the prominent feature is splitting of the main peaks ( $A_1$ - $A_4$ ) into two peaks (squares and circles). With the increase of  $\theta_x$  (angle of rotation along the x-axis), these peaks behave differently depending on the value of H. In the case of sample 1 (Fig. 5a), the longer wavelength peak undergoes further red shift with  $\theta_x$  (squares) while the amount of blue shift of

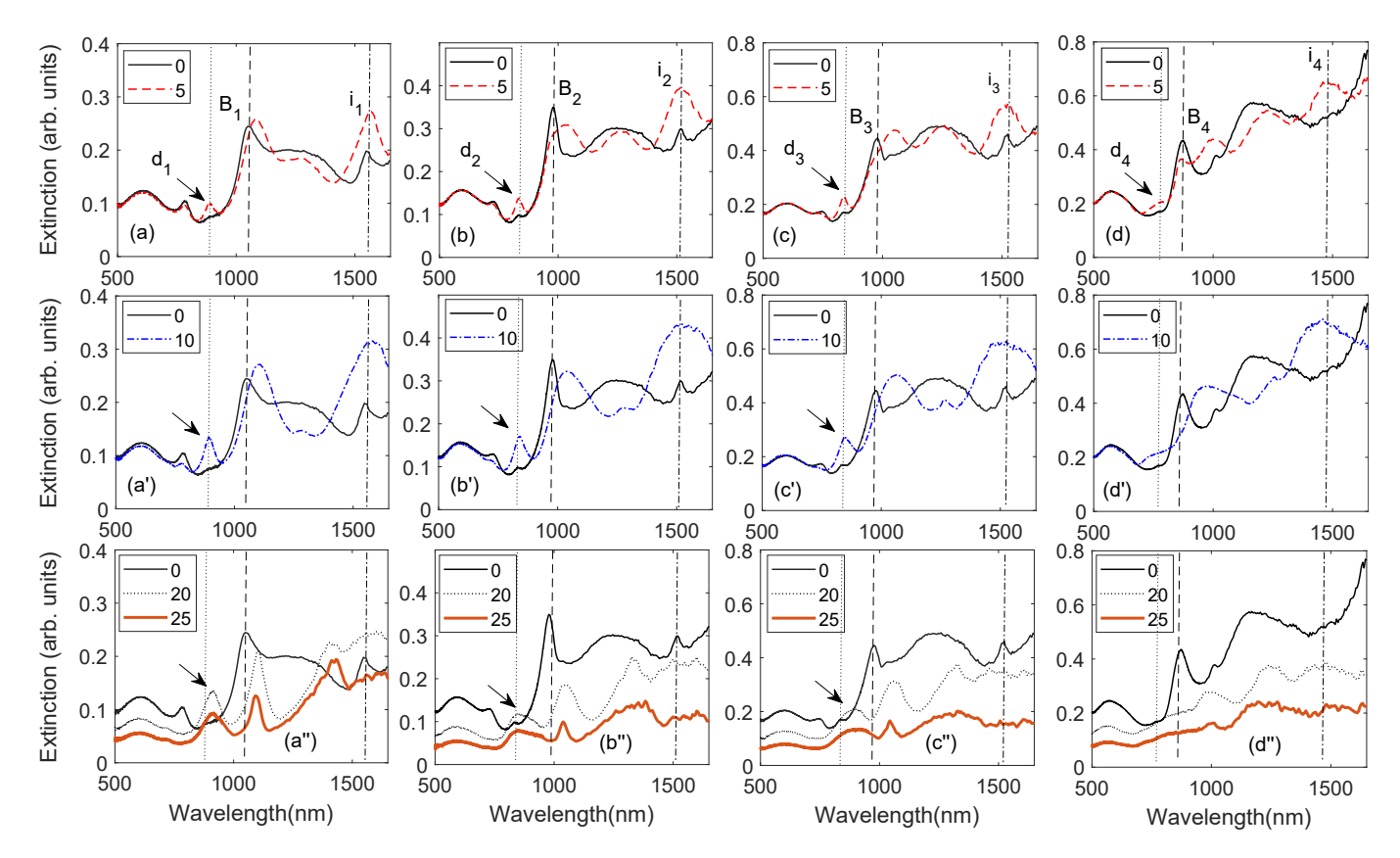


**Fig. 4.** Extinction spectra of samples 1(a-a''), 2(b-b''), 3(c-c''), and 4(d-d'') when the samples are rotated along the y-axis and the incident light is polarized along x-axis. The legends refer to the angle of rotation  $(\theta_y)$ . The vertical dotted, dashed, and dashed-dotted lines, highlight the wavelengths of dark, main, and infrared peaks, respectively.

the shorter wavelength peak is less significant (circles). Similar features can be seen for the case of sample 2 (Fig. 5b), although here the blue shift of the shorter wavelength peak becomes more distinct (circles). Samples 3 and 4 indicate that with the increase of  $\theta_X$ , in addition to shifts of the two satellites (squares and circles) associated with main peak (A<sub>3</sub> add A<sub>4</sub>), peaks c<sub>3</sub> and c<sub>4</sub> undergo red shift (pluses). As a result, the peaks at 680 and 637 nm in Fig. 5c and d when  $\theta_X = 15^\circ$  can be associated with the overlaps of these two contributions. Further increase of  $\theta_X$  removes such a degeneracy (Fig. 5d) [39].

The results seen in Fig. 5 can be explained considering coupling of the plasmon modes of individual FmANTs with RA. The wavelength of the first order RA can be obtained using  $\lambda_{RA} = a(n \pm \sin(\theta_x))$  wherein a refers to the lattice constants  $(a_x \text{ or } a_y)$ and n is the refractive index of the substrate or superstrate. This equation highlights the two associated modes of RA, i.e.  $m = \pm 1$  (mis the order of diffraction). For  $\theta_x=0^\circ$ , the two modes (+1,0) and (-1,0) are degenerate. Considering these, we associate peaks  $A_1$ - $A_4$ with the SLRs caused by coupling of the edge modes with RA in the substrate. This can be related with the fact that for refractive index of glass (1.51) and  $a_y = 500$ ,  $\lambda_{RA}$  becomes 755 nm. This is further confirmed by the fact that variation of peaks A<sub>1</sub>-A<sub>4</sub> with variation of refractive index of the superstrate is rather small (Fig. 2 with air or methanol), indicating optical diffraction mostly occurs in the substrate. Our results indicate that as H increases the difference between the wavelength of these peaks and the RA wavelength reduces, leading to a stronger coupling. The mode (+1,0) is a standard mode associated with the bright mode of plasmons. For (-1,0), however, for  $\theta_x = 0^\circ$ , the plasmon modes are dark. With increase of  $\theta_x$ , they are coupled to the lattice modes while blue shifted. Our results show that for sample 1, the (-1,0) mode seems

to be close to the continuum of states. The impact of such plasmon modes can become more visible in the case of samples 3 and 4 wherein we see the peaks at 600 nm, which might be associated with edge modes under y-pol, undergo significant red shift with rotation of samples (pluses). This process can obscure the wavelength shift of (+1,0). As shown in the Supporting Information (Fig. S3), if we keep the polarization of the incident light along y-axis but rotate the samples along y-axis, no doubling occurs.

## 4. Polarization switching of in-plane light scattering

Under the conditions where SLR occurs one expects the light diffraction along the plane of the array to present distinct features. Such a process should depend on the shapes (flatness) and polarizability of the FmANTs. To inspect these features, we spectrally and spatially analyzed the in-plane light scattering using an optical setup as shown in Fig. 1c. For this, we rotated the polarization of the incident light, making angle  $\beta$  with respect to x-axis. Therefore, for  $\beta=0^{\circ}$ , we have x-pol and  $\beta=90^{\circ}$  refers to y-pol. With this, the microscope objective 1 was moved parallel to the x-axis (Fig. 1c). Evolution of the light reaching this objective for different values of x, distance from one edge of the substrate, for sample 1 (Fig. 1c) are shown in Fig. S4 of the Supporting Information. The results show that when x, i.e. the distance of objective 1 from the corner edge of the sample (Fig. 1c), is 5 mm, the intensity of the detected light reaches a maximum before it starts to decrease as x increases further. This shows that the scattering field reaches the edge of the substrate in a finite spatial range. Fig. 6 presents the results of spectral variation of the in-plane light scattering for sample 1 (a), 2 (b), 3 (c), and 4 (d) when x = 5 mm and the axis of polarization of the incident light is rotated by  $\beta$ . For the case of sample 1, the results

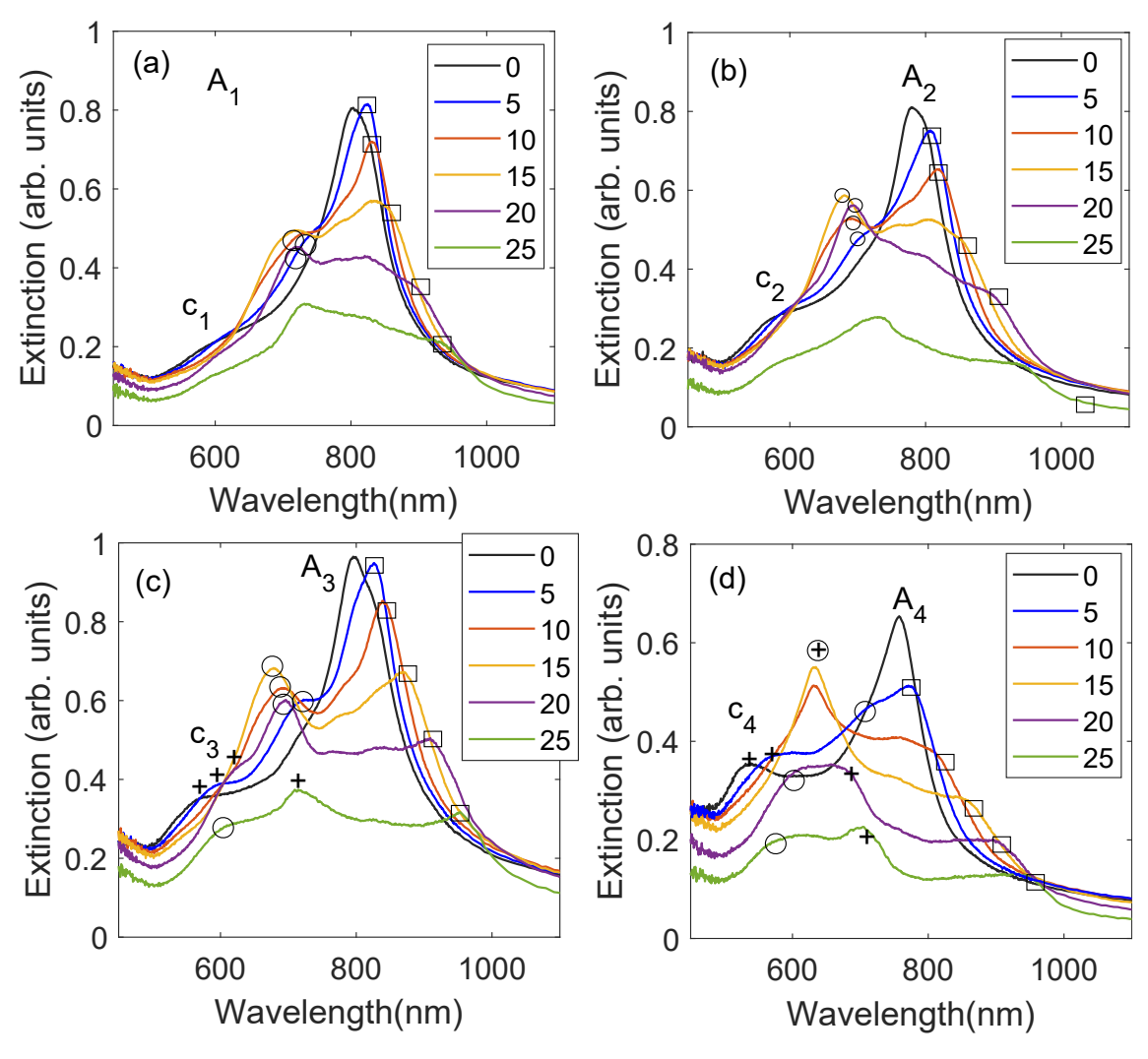


**Fig. 5.** Extinction spectra of samples 1 (**a**), 2 (**b**), 3 (**c**), and 4 (**d**) when the samples are rotated along the x-axis and the incident light is polarized along y-axis. The legends refer to the angle of rotation in degrees ( $\theta_x$ ).

show some interesting spectral transition. For  $\beta=0^\circ$  (x-pol), we can see two peaks, a weak one at about 777 nm (peak 1) and a much stronger one at about 891 nm (peak 2). This suggests that when the FmANTs with H = 20 nm are excited along the x-axis, majority of light at location x = 5 mm is concentrated at 891 nm. As  $\theta$  increases (legend), peak 2 starts to diminish while peak 1 becomes dominant. In fact for  $\beta=90^\circ$ , peak 1 increases by about 10 times without significant change in its central wavelength.

The results shown in Fig. 6 suggest that as H increases the inplane light scattering changes dramatically. For case of sample 2 (Fig. 6b), similar to the case of sample 1, when  $\beta=0^\circ$ , we can see a spectrum consisted of two peaks (peak 1 at 760 nm and peak 2 at 871 nm). In contrast to the case of H = 20 nm (sample 1), however, as  $\beta$  changes from  $0^\circ$  (x-pol) to  $90^\circ$  (y-pol), in this sample peak 1 does not change significantly in amplitude. Rather peak 2 becomes more dominant as it is blue shifted. A similar trend is observed for the case of samples 3 and 4. For these samples, peaks 2 seem to become the dominant peaks when  $\beta=90^\circ$  and variation of  $\theta$  does not lead to a large relative increase of the peak amplitudes. The results also show that with increase of H, several extra peaks are formed on the right side of peak 2 (peaks 3 and 4 in the case of sample 4). These peaks are dominantly seen in the case of  $\beta=0^\circ$ . They disappear as the  $\beta$  reaches  $90^\circ$ .

The results in Fig. 7 shows variations of the spectra of the scattered light from the edge of sample 1 (x) for  $\beta=0^\circ$  (Fig. 7a),  $\beta=30^\circ$  (Fig. 7b), and  $\beta=90^\circ$  (Fig. 7c). One can see here that for the cases (Fig. 7a) and (Fig. 7c), we mostly see intensity variations, as spectra remain nearly unchanged at different locations at the edge. For the case of  $\beta=30^\circ$ , however, as x increases the rise of intensity occurs with distinct spectral variations. For low x, it seems the longer wavelength peak has a slightly higher amplitude. At x=5 mm, the two distinct peaks with nearly the same amplitudes emerges. As x increases further significant reduction of intensity occurs with relative increase of the shorter wavelength peak amplitude. These results suggest that for certain polarization axes of the incident light, light diffraction at different directions can be quite different.

These results can be related to those presented in Fig. 2, wherein for x-pol, we saw the formation of several peaks associated with multipolar nature of plasmon edge modes. For y-pol, however, Fig. 2 shows two dominant peaks (c's and A's). Considering the fact for y-pol, we mostly deal with SLR, and for x-pol, the incident light dominantly excite the longitudinal edge modes of the nanoantennas, the results in Fig. 6 demonstrate a pronounced transition from plasmon scattering by individual nanoantennas to collective diffraction by SLR, as  $\beta$  changes from 0° to 90°. Such a polarization

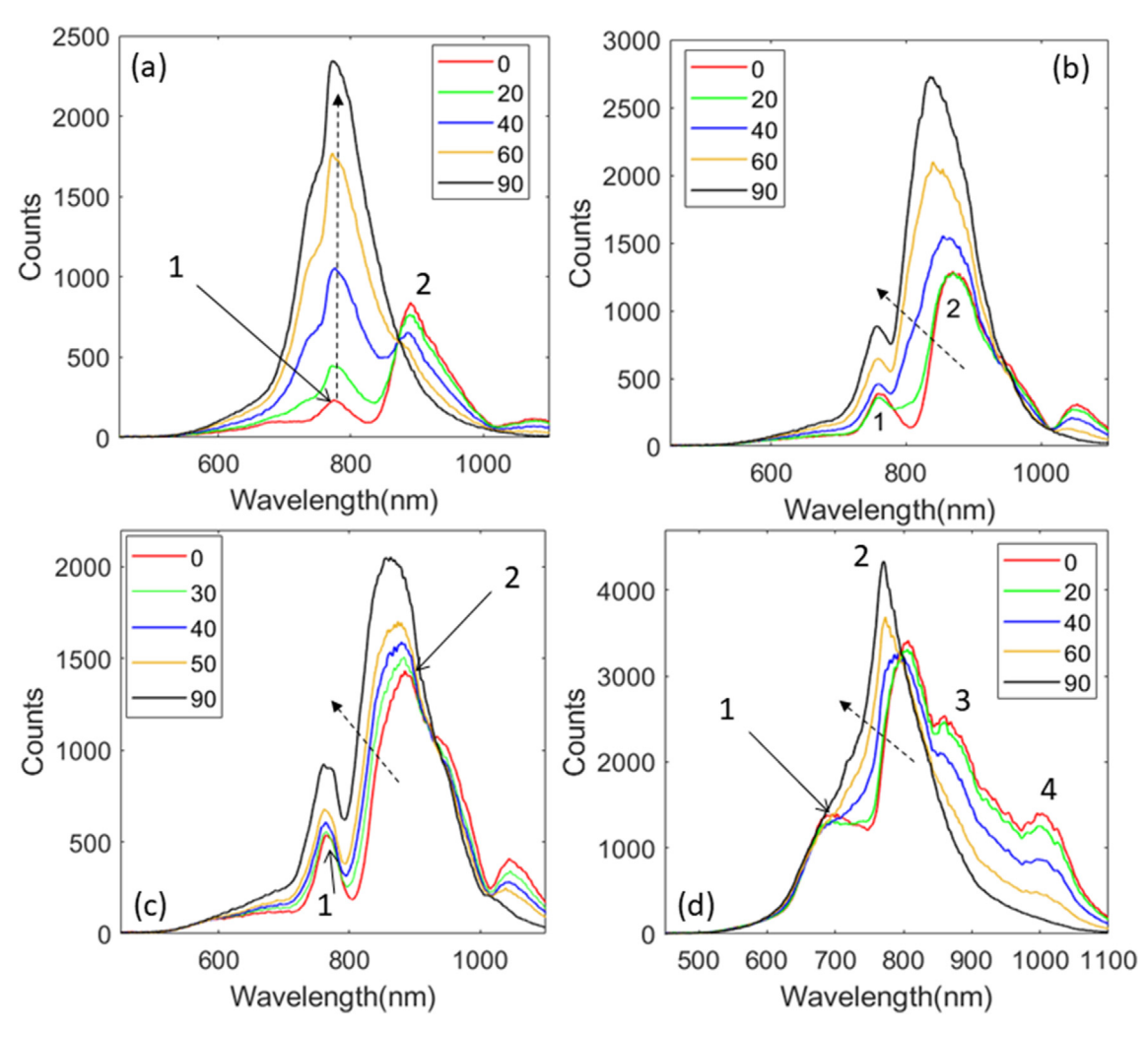


**Fig. 6.** (a), (b), (c), (d) In-plane light scattering at x = 5.0 mm for sample 1–4 ((a)–(d)). The legend refers to the value of β, i.e. angle of polarization axis of incident light. The dashed arrows show the trend of variation of spectra with the increase of β.

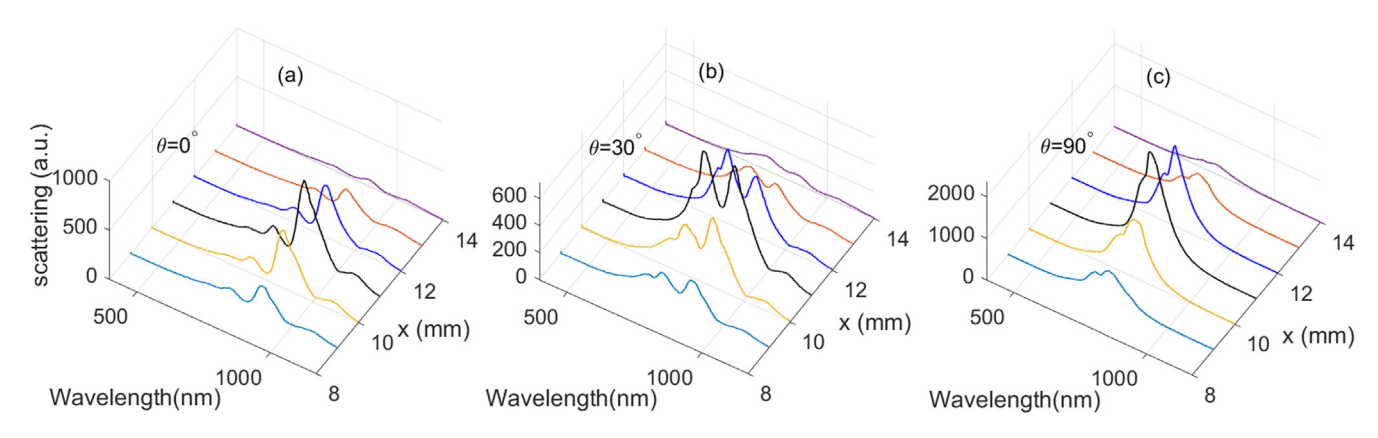


**Fig. 7.** Spectral variation of the scattered light from the edge of sample 1 as a function of x for  $\beta=0^\circ$  (a),  $\beta=30^\circ$  (b),  $\beta=90^\circ$  (c).

switching process can be further analyzed considering the contour plots of the results shown in Fig. 6. As seen in Fig. 8a, in the case of sample 1, we can see a clear switching between peak 1 and peak 2 when  $\beta \sim 10^{\circ}$ . There is little overlap between plasmonic and collective scattering. In the case of samples 2–4, however, the transition between these two processes does not happen with an abrupt wavelength change, rather we have mixing of edge modes

and SLR. These results suggest that sample 1, i.e. FmANTs with a high degree of flatness, can funnel energy into a specific wavelength range and at a given location at the edge of the sample as  $\beta$  reaches 90°. These results suggest an optical switching process controlled by the incident light polarization. As H increases, as seen in Fig. 8b–d, the transition between plasmonic scattering and diffraction becomes continuous. Note that the timescale of the

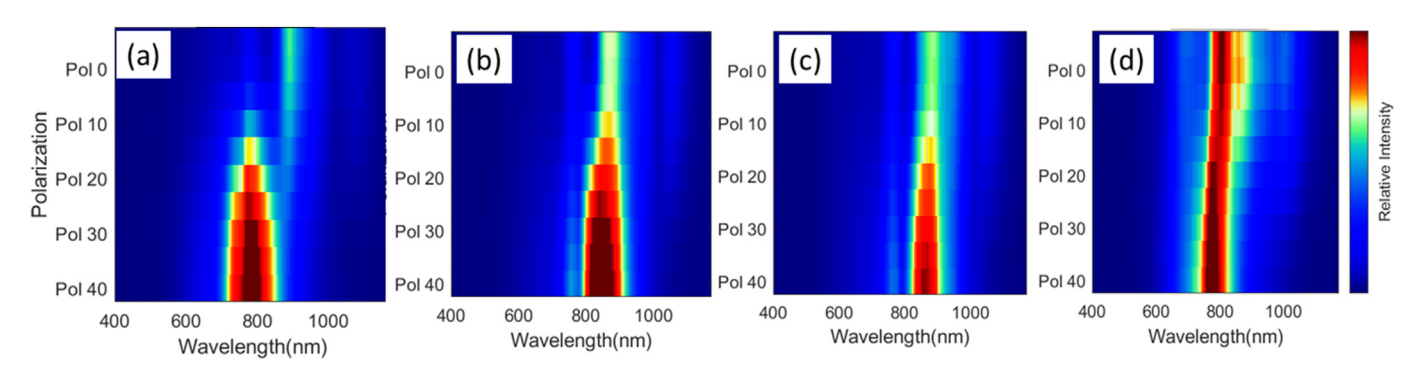


Fig. 8. Contour plots associated with the results shown in Fig. 6. Here (a)–(d) refer to the samples 1–4, respectively.

switching process studied here is limited by the plasmon excitation responses of the FmANTs, which are shown to be very fast [40].

Note that the subject of light diffraction via arrays of metallic nanoantennas and its diverse applications have been studied in the past extensively [1–14]. A recent report, in particular, has utilized in-plane light scattering in such arrays to investigate SLR lasers and their applications to identify photonics Brillouin zones and the radiated electromagnetic fields from edges of these zones [41]. This report has shown the in-plane lasing beams can show signatures of the symmetry points in the first or higher order Brillouin zones. Additionally, recently the study by Karabchevsky et al. [34] has reported a polarization switch based on the excitation of molecular overtone transitions in a hybrid plasmonic—dielectric configuration. In this system, guided wave plasmons were used.

#### 5. Conclusions

We studied control of in-plane light scattering in periodic arrays of metallic nanoantennas with heights much less than their lateral sizes. Our results showed that such arrays can offer unique features when the degrees of their flatness become high. These include the polarization-dependent partition of in-plane scattering into two modes with quite different spectral wavelengths. The switching process occurs as the polarization of the incident light is rotated, allowing transfer of incident light energy into far-field scattering associated with the localized edge-mode plasmon modes or with the coherence scattering supported by the SLRs formed via coherent optical coupling of such edge-mode plasmons. The outcomes show the unique aspects of ultra-flat nanoantennas with potential applications in integrated photonic devices, laser systems, spectroscopic systems, and sensors.

## Credit author statement

Seyed Sadeghi: Analysis, Writing, Conceptualization, Graphics Rithvik Gutha: Fabrication, Measurements, Optical Setup, Characterization Sean Ramsay: Data Collection, Optical scattering Measurements Dustin Robert: Optical setup Christina Sharp: Optical Measurement, Characterization.

## **Declaration of competing interest**

The authors declare that they have no known competing financial interests or personal relationships that could have appeared to influence the work reported in this paper.

## Acknowledgments

This work is supported by the US National Science Foundation under grant ECCS-1917544.

### Appendix A. Supplementary data

Supplementary data to this article can be found online at https://doi.org/10.1016/j.mtnano.2022.100190.

#### References

- [1] V.G. Kravets, A.V. Kabashin, W.L. Barnes, A.N. Grigorenko, Chem. Rev. 118 (2018) 5912.
- [2] S.R.K. Rodriguez, A. Abass, B. Maes, O.T. Janssen, G. Vecchi, J.G. Rivas, Phys. Rev. X 1 (2011), 021019.
- [3] S.M. Sadeghi, W.J. Wing, R.R. Gutha, J. Opt. 23 (2021), 025003.
- [4] R.R. Gutha, S.M. Sadeghi, C. Sharp, W.J. Wing, Nanotechnology 28 (2017) 355504.
- [5] X. Zhang, S. Feng, J. Zhang, T. Zhai, H. Liu, Z. Pang, Sensors 12 (2012) 12082.
- [6] B.D. Thackray, V.G. Kravets, F. Schedin, G. Auton, P.A. Thomas, A.N. Grigorenko, ACS Photonics 1 (2014) 1116.
- [7] B. Auguié, W.L. Barnes, Phys. Rev. Lett. 101 (2008) 143902.
- 8] S.M. Sadeghi, W.J. Wing, Q. Campbell, J. Appl. Phys. 119 (2016) 244503.
- [9] S.M. Sadeghi, R.R. Gutha, W.J. Wing, Opt Lett. 41 (2016) 3367.
- [10] R. Guo, S. Derom, A. Väkeväinen, R. van Dijk-Moes, P. Liljeroth, D. Vanmaekelbergh, P. Törmä, Opt Express 23 (2015) 28206.
- [11] M. Ramezani, G. Lozano, M.A. Verschuuren, J. Gómez-Rivas, Phys. Rev. B 94 (2016) 125406.
  [12] X. Yuan, L. Shi, Q. Wang, C. Chen, X. Liu, L. Sun, B. Zhang, J. Zi, W. Lu, Opt
- Express 22 (2014) 23473. [13] R.R. Gutha, S.M. Sadeghi, C. Sharp, A. Hatef, Y. Lin, J. Appl. Phys. 125 (2019),
- 023103. [14] N. Liu, M. Mesch, T. Weiss, M. Hentschel, H. Giessen, Nano Lett. 10 (2010)
- [15] R.J. Bettles, S.A. Gardiner, C.S. Adams, Phys. Rev. Lett. 116 (2016) 103602.
- [16] S.M. Sadeghi, R.R. Gutha, Physical Review Applied 15 (2021), 034018.
- [16] S.M. Sadeghi, R.R. Gutha, Physical Review Applied 15 (2021), 034018 [17] S.M. Sadeghi, R.R. Gutha, Applied Materials Today 22 (2021) 100932.
- [18] V. Giannini, G. Vecchi, J.G. Rivas, Phys. Rev. Lett. 105 (2010) 266801.
- [19] E.P. Bellido, A. Manjavacas, Y. Zhang, Y. Cao, P. Nordlander, G.A. Botton, ACS Photonics 3 (2016) 428.
- [20] A. Campos, A. Arbouet, J. Martin, D. Gerard, J. Proust, J. Plain, M. Kociak, ACS Photonics 4 (2017) 1257.
- [21] E.P. Bellido, Y. Zhang, A. Manjavacas, P. Nordlander, G.A. Botton, ACS Photonics (2017), https://doi.org/10.1021/acsphotonics.7b00348, 0.
- [22] F.-P. Schmidt, H. Ditlbacher, A. Hohenau, U. Hohenester, F. Hofer, J.R. Krenn, Nano Lett. 16 (2016) 5152.
- [23] F.-P. Schmidt, H. Ditlbacher, U. Hohenester, A. Hohenau, F. Hofer, J.R. Krenn, Nat. Commun. 5 (2014).
- [24] S.M. Sadeghi, W.J. Wing, R.R. Gutha, C. Sharp, A. Hatef, J. Appl. Phys. 122 (2017), 063102.
- [25] R.R. Gutha, S.M. Sadeghi, A. Hatef, C. Sharp, Y. Lin, Appl. Phys. Lett. 112 (2018) 223102.
- [26] S.M. Sadeghi, R.R. Gutha, W.J. Wing, C. Sharp, L. Capps, C. Mao, J. Phys. Appl. Phys. 50 (2017) 145401.
   [27] V.J. Keast, C. Walhout, T. Pedersen, N. Shahcheraghi, M. Cortie, D.R. Mitchell,
- [27] V.J. Keast, C. Walhout, T. Pedersen, N. Shahcheraghi, M. Cortie, D.R. Mitchel Plasmonics 11 (2016) 1081.
- [28] K. Imaeda, S. Hasegawa, K. Imura, J. Phys. Chem. C 122 (2018) 7399.
- [29] E.P. Bellido, G.D. Bernasconi, D. Rossouw, J. Butet, O.J. Martin, G.A. Botton, ACS Nano 11 (2017) 11240.
- [30] I.C. Bicket, E.P. Bellido, D.M. McRae, F. Lagugné-Labarthet, G.A. Botton, ACS Photonics 7 (2020) 1246.
- [31] X. Lu, Q. Hao, M. Cen, G. Zhang, J. Sun, L. Mao, T. Cao, C. Zhou, P. Jiang, X. Yang, et al., Nano Lett. 18 (2018) 2879.
- [32] J.K. El-Demellawi, S. Lopatin, J. Yin, O.F. Mohammed, H.N. Alshareef, ACS Nano 12 (2018) 8485.
- [33] J. Guan, L.K. Sagar, R. Li, D. Wang, G. Bappi, W. Wang, N. Watkins, M.R. Bourgeois, L. Levina, F. Fan, et al., ACS Nano 14 (2020) 3426.

- [34] A. Karabchevsky, A. Hazan, A. Dubavik, Adv. Opt. Mater. 8 (2020) 2000
- [35] T.C. Tan, E. Plum, R. Singh, Photonics, 6, Multidisciplinary Digital Publishing
- [35] I.C. Tali, E. Pililli, K. Shigli, Photonics, 6, Multidisciplinary Digital Publishing Institute, 2019, p. 75.
  [36] M.W. Knight, J. Fan, F. Capasso, N.J. Halas, Opt Express 18 (2010) 2579.
  [37] J.A. Fan, K. Bao, J.B. Lassiter, J. Bao, N.J. Halas, P. Nordlander, F. Capasso, Nano Lett. 12 (2012) 2817.
- [38] E. Babich, S. Scherbak, F. Heisler, S. Chervinskii, A. Samusev, A. Lipovskii, Journal of Physics: Conference Series, vol. 769, IOP Publishing, 2016, p. 12040.
- [39] R.R. Gutha, S.M. Sadeghi, C. Sharp, W.J. Wing, J. Phys. Appl. Phys. 51 (2018), 045305.
- [40] S.K. Cushing, N. Wu, J. Phys. Chem. Lett. 7 (2016) 666.
  [41] J. Guan, M.R. Bourgeois, R. Li, J. Hu, R.D. Schaller, G.C. Schatz, T.W. Odom, ACS Nano 15 (2021) 5567.